Journal of Hepatocellular Carcinoma

Dovepress
Taylor & Francis Group

Open Access Full Text Article

ORIGINAL RESEARCH

MRI Radiomics to Predict Early Treatment Response to TACE Combined with Lenvatinib Plus a PD-1 Inhibitor for Hepatocellular Carcinoma with Portal Vein Tumor Thrombus

Deyu Lu[1], Lingling Zhou[2], Ziyi Zuo[3], Zhao Zhang[4], Xiangwu Zheng[4], Jialu Weng[1], Zhijie Yu[1], Jiansong Ji[2,5], Jinglin Xia[1,6,7]

[1]Zhejiang Key Laboratory of Intelligent Cancer Biomarker Discovery and Translation, The First Affiliated Hospital of Wenzhou Medical University, Wenzhou, 325035, People's Republic of China; [2]Key Laboratory of Imaging Diagnosis and Minimally Invasive Intervention Research, Institute of Imaging Diagnosis and Minimally Invasive Intervention Research, The Fifth Affiliated Hospital of Wenzhou Medical University, Lishui Hospital of Zhejiang University, Lishui, 323000, People's Republic of China; [3]Division of Pulmonary Medicine, The First Affiliated Hospital of Wenzhou Medical University, Wenzhou Key Laboratory of Interdiscipline and Translational Medicine, Wenzhou Key Laboratory of Heart and Lung, Wenzhou, Zhejiang, 325000, People's Republic of China; [4]Department of Radiology, The First Affiliated Hospital of Wenzhou Medical University, Wenzhou, 325000, People's Republic of China; [5]Clinical College of The Affiliated Central Hospital, School of Medicine, Lishui University, Lishui, 323000, People's Republic of China; [6]Liver Cancer Institute, Zhongshan Hospital of Fudan University, Shanghai, 200032, People's Republic of China; [7]National Clinical Research Center for Interventional Medicine, Zhongshan Hospital of Fudan University, Shanghai, 200032, People's Republic of China

Correspondence: Jinglin Xia, Zhejiang Key Laboratory of Intelligent Cancer Biomarker Discovery and Translation, The First Affiliated Hospital of Wenzhou Medical University, Nanbaixiang Street, Ouhai District, Wenzhou, 325035, People's Republic of China, Email xiajinglin@fudan.edu.cn; Jiansong Ji, Key Laboratory of Imaging Diagnosis and Minimally Invasive Intervention Research, Institute of Imaging Diagnosis and Minimally Invasive Intervention Research, The Fifth Affiliated Hospital of Wenzhou Medical University, Lishui Hospital of Zhejiang University, 289 Kuocang Road, Lishui, 323000, People's Republic of China, Email jjstcty@wmu.edu.cn

Purpose: To develop and validate a predictor for early treatment response in hepatocellular carcinoma (HCC) patients accompanied by portal vein tumor thrombus (PVTT) undergoing transarterial chemoembolization (TACE), lenvatinib and a programmed cell death protein 1 (PD-1) inhibitor (TLP) therapy.

Patients and Methods: In this retrospective study, patients with HCC and PVTT from two institutions receiving triple TLP therapy were enrolled. Radiomics features derived from pretreatment contrast-enhanced MRI were curated using intraclass correlation coefficient (ICC), Student's *t*-test, least absolute shrinkage and selection operator (LASSO), and recursive feature elimination (RFE) to ensure robust selection. Various machine learning (ML) algorithms were then used to construct the models. The meaningful clinical indicators were obtained via logistic regression analysis and ultimately integrated with radiomics features to develop a combined model. In addition, we used Shapley Additive exPlanation (SHAP) to clarify the model's operational dynamics.

Results: Our study ultimately included 115 patients (7:3 randomization, 80 and 35 in the training and test cohorts, respectively) in total. No patients achieved complete remission, 47 achieved partial remission, 29 achieved stable disease, and 39 experienced disease progression. Among objective response rates (ORRs) and disease control rates (DCRs), 40.9% and 66.1% were reported. One of the four ML classifiers with optimal performance, namely random forest, was adopted as the radiomics model after testing. Regarding the performance assessment, the radiomics model's area under the curve (AUC) values reached 0.92 (95% CI: 0.86–0.97) and 0.79 (95% CI: 0.61–0.95), inferior to the combined model's AUCs of 0.95 (95% CI: 0.68–0.98) and 0.84 (95% CI: 0.91–0.99). Moreover, the SHAP plots illustrate the importance of global variables and the prediction process for individual samples.

Conclusion: The model based on machine learning and radiomics showed favorable performance, and the operating mode was visualized through SHAP.

Keywords: radiomics, HCC, portal vein tumor thrombus, lenvatinib, immune checkpoint inhibitor

Received: 14 January 2025
Accepted: 8 May 2025
Published: 16 May 2025

Introduction

Hepatocellular carcinoma (HCC), a significant global health challenge, ranks sixth among the most common cancers and is the third highest cause of cancer-related mortality. Globocan's latest statistics report nearly 865,000 new cases and approximately 758,000 fatalities each year.[1]

The majority of HCC patients present at intermediate to advanced stages, often with PVTT, which occurs in 44.0–62.2% of cases and is associated with poor treatment response and prognosis.[2] In Europe and the United States, this patient population, classified as Barcelona Clinic Liver Cancer (BCLC) stage C, is managed with systemic therapy, encompassing immune checkpoint inhibitors and tyrosine kinase inhibitors.[3,4] However, transarterial chemoembolization (TACE) remains the preferred initial therapy for patients afflicted with HCC plus PVTT (HCC-PVTT) in China, without extrahepatic metastases.[5] Although TACE alone or in combination with other therapies has improved overall survival among HCC-PVTT patients.[6–8] the efficacy and prognosis vary widely among individuals.

First conceptualized by Lambin in 2012,[9] radiomics has evolved into a robust methodology for quantitative feature extraction from medical images, demonstrating substantial scientific progress over the past decade. Since deep image features may reflect tumor biological behavior and heterogeneity,[10] researchers have integrated those features with artificial intelligence algorithms to develop models for solving medical problems.[11–13]

Lenvatinib, a multikinase inhibitor, selectively targets multiple angiogenesis-associated signaling pathways, thereby potently inhibiting tumor neovascularization.[14] Concurrently it exerts its therapeutic effects by directly suppressing tumor cell proliferation and regulating tumor immune microenvironment. Owing to these synergistic pharmacological properties, lenvatinib has emerged as a frontline treatment for advanced HCC,[2–4] but its clinical benefit is limited by tumor heterogeneity and chemoresistance. Consequently, Bo et al sought to forecast the effectiveness of lenvatinib monotherapy in unresectable HCC on the basis of contrast-enhanced CT images.[11] They analyzed cases from three medical centers and obtained information from CT images. The machine learning (ML) radiomics model had an AUC of 0.97 and achieved satisfactory results in the external validation cohort. Pretreatment MRI radiomics features combined with clinical variables could aid in clinical decision-making in identifying potential beneficiaries among advanced HCC patients receiving lenvatinib plus TACE therapy.[15] Recently, a retrospective study confirmed the predictive value of radiomics for survival and therapeutic response in unresectable HCC patients treated with systemic therapy plus endovascular intervention.[13] Furthermore, Cheng and colleagues developed a convenient, noninvasive and individualized assessment tool for patients with HCC and PVTT on the basis of radiomics features and clinical indicators.[16]

Numerous radiomics investigations have focused on HCC and PVTT; however, scant research has addressed the prognosis of HCC-PVTT patients undergoing multidisciplinary treatment. Therefore, our objective was to develop a radiomics model based on pretreatment contrast-enhanced MRI to forecast the short-term efficacy of TACE plus lenvatinib and programmed cell death protein 1 (PD-1) blockade (TLP) triple therapy in HCC-PVTT patients.

Materials and Methods

Patient Selection

We enrolled 249 hCC-PVTT patients receiving triple TLP therapy from two institutions, comprising 206 cases at the First Affiliated Hospital of Wenzhou Medical University (February 2021-July 2024) and 43 cases at the Fifth Affiliated Hospital of Wenzhou Medical University (March 2021-March 2023). The participants in this study met the following criteria: (1) age 18–85 years, with no sex restrictions; (2) HCC with PVTT diagnosed by radiology or histopathology; (3) availability of contrast-enhanced MRI scans pre- and post-treatment (1 month and 3–4 months); (4) Child-Pugh A/B liver function and Eastern Cooperative Oncology Group performance status (ECOG-PS) scores of 0–2; (5) allowance for prior radical hepatectomy/ablation within 3 months pre-enrollment; (6) demonstrated regular follow-up compliance. The exclusion criteria comprised: (1) concomitant with other malignancies; (2) extrahepatic metastases; (3) prior antitumor therapies (ie, liver transplantation, radiotherapy, TACE, or systemic therapy); (4) absence of measurable target lesions; (5) incomplete clinical/MRI data. We divided PVTT into four types via Cheng's classification system: type I involves intra-lobar portal vein branches; type II involves the left or right portal vein branches; type III involves the main portal vein; and type IV denotes superior mesenteric vein

invasion.[17] Patients were allowed to receive different anti-PD-1 strategies, in accordance with real-world practice, and previous studies have shown no effect of the PD-1 inhibitor category on antitumor efficacy.[18]

Contrast-Enhanced MRI data were procured in digital imaging and communications in medicine (DICOM) format for subsequent analysis. Moreover, the relevant demographic and clinical information was obtained from the electronic medical record system, as shown in Figure 1. The systemic immune-inflammation index (SII) (calculated as platelet × neutrophil / lymphocyte counts) and the albumin-bilirubin (ALBI) score [–0.085 × albumin (g/L) + 0.66 × log10 bilirubin (μmol/L)] were utilized to evaluate immune-inflammatory status and hepatic function, respectively.

Treatment Protocol

Eligible patients received oral lenvatinib (8 mg/day <60 kg, 12 mg/day ≥60 kg) and anti-PD-1 immunotherapy (tislelizumab 200 mg, sintilimab 200 mg, camrelizumab 200 mg, pembrolizumab 200 mg, penpulimab 200 mg, and cadonilimab 375 mg) every 3 weeks. Treatment was adjusted or discontinued when disease progression or intolerable adverse events occurred. Seasoned interventional radiologists executed the TACE procedure within the combined therapy regimen. Utilizing the modified Seldinger technique, they initially accessed the right femoral artery and employed selective angiography to pinpoint the tumor-feeding artery. Subsequently, a microcatheter was precisely navigated to the target vessel for the infusion of chemotherapeutic agents combined with lipiodol (1 to 30 mL) or drug-eluting beads (DEBs) (loaded with epirubicin at a dose of 30 or 50 mg, with diameters of 100–300 μm and 300–500 μm). Embolization was completed with a gelatin sponge or microspheres until arterial stasis was achieved. The chemotherapeutic agents administered included pirarubicin (10–30 mg), epirubicin (10–50 mg), mitomycin (10 mg), oxaliplatin (50–150 mg), raltitrexed (1–4 mg), and 5-fluorouracil (250–1000 mg).

Tumor Response Evaluation

Following the modified Response Evaluation Criteria in Solid Tumors (mRECIST),[19] tumor responses—complete response (CR), partial response (PR), progressive disease (PD), and stable disease (SD)—were evaluated 3–4 months post-initial treatment. The objective response rate (ORR) denotes patients attaining CR or PR, while the disease control rate (DCR) encompasses those with SD, PR, or CR.

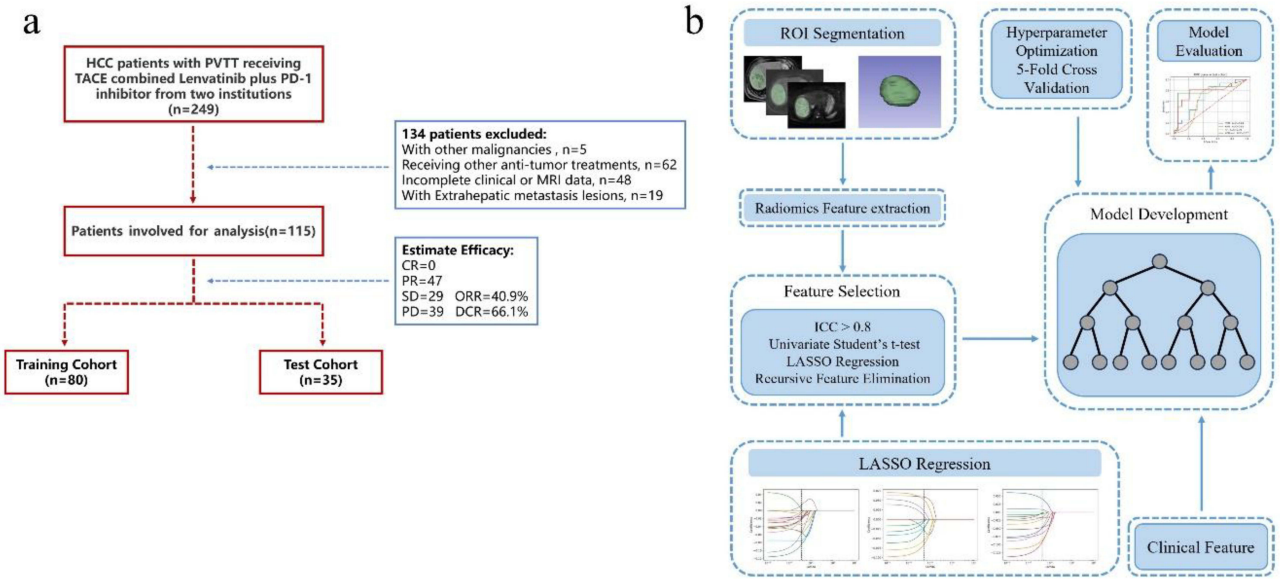

Figure 1 Flowchart of the study. (**a**) Flowchart of patient selection. Cases meeting the inclusion and exclusion criteria were retrospectively collected from two institutions and allocated into the training and test cohorts at a 7:3 ratio. (**b**) Flowchart of development and validation of evaluation models. Radiomics features were extracted from manually segmented ROIs. Predictive features were subsequently selected through ICC analysis, Student's *t*-test, LASSO regression and RFE. Clinical indicators were incorporated to establish the combined model. Following hyperparameter optimization, the model with the optimal parameters underwent performance evaluation.

https://doi.org/10.2147/JHC.S513696

MRI Examination Procedure

All participants completed protocol-mandated pre-procedural fasting (6–8h) prior to MRI. MRI images were acquired using 1.5T/3.0T scanners: [1.5T] uMR586/680 (United Imaging Healthcare, Shanghai, China); Aera/Avanto/Symphony Tim (Siemens Healthcare, Erlangen, Germany); Signa HDxt/HDe/Voyager (GE Healthcare, Milwaukee, WI, USA); [3.0T] Prisma/Skyra (Siemens Healthcare, Erlangen, Germany); Discovery MR750/Signa HDxt (GE Healthcare, Milwaukee, WI, USA); Achieva/Ingenia ElitionX (Philips Medical Systems, Best, Netherlands), with protocol-specific sequences/parameters detailed in Supplementary Table S1. Arterial, portal, and delayed phase images were obtained at 15–20, 50–55, and 85–90 seconds after intravenous injection of gadodiamide (Omniscan 0.5 mmol/mL; GE Healthcare), respectively. Contrast agent injection was followed by irrigation with 20 mL of normal saline. Selected for analysis were arterial phase T1-weighted imaging (T1WI), T2-weighted imaging (T2WI), and diffusion-weighted imaging (DWI) with b values of 600 or 800 s/mm^2.

ROI Segmentation and Radiomics Feature Extraction

MRI image preprocessing was performed before region of interest (ROI) segmentation to improve stability and repeatability,[20] involving N4 bias field correction,[21] MRI signal intensity normalization via the z-score method and voxel resampling (3×3×3 mm). Two radiologists used a 3D slicer (version 5.4.0; www.slicer.org) to segment the ROI layer by layer and then fused it to form a three-dimensional structure. For patients with multiple HCC lesions, the largest lesion was selected. During ROI segmentation, the radiologist was blinded to the patient's clinical information. Radiomics features were extracted via radiomics extension modules on a 3D slicer. We obtained 851 features from each sequence, including 14 shape features, 18 first-order statistical features, 14 gray level dependence matrix (GLDM), 24 gray level co-occurrence matrix texture (GLCM), 16 gray level size zone matrix (GLSZM), 16 gray level run length matrix (GLRLM), 5 neighboring gray tone difference matrix (NGTDM), and 744 wavelet transformed features.

Feature Selection

Interobserver agreement of radiomics features was assessed by intraclass correlation coefficient (ICC), and only features with an ICC > 0.8 were retained for subsequent analysis. Feature dimensionality reduction was achieved via Student's *t*-test and least absolute shrinkage with selection operator (LASSO) algorithms, validated through 10-fold cross-validation. Finally, we adopted recursive feature elimination (RFE) based on logistic regression to filter again after feature summarization. In addition, we employed univariate analysis to discern potential clinical variables and conducted multivariate logistic regression on those with a p value <0.05.

Prediction Model Construction and Evaluation

A synthetic minority oversampling technique (SMOTE) was employed to overcome the data imbalance in the training cohort. Four classifiers were applied to train the radiomics models, namely, support vector machine (SVM), k-nearest neighbor (KNN), random forest (RF), and eXtreme gradient boosting (XGBoost). To prevent overfitting and enhance model generalizability, a grid search with 5-fold cross validation was employed to determine the optimal classifier parameters (Supplementary Table S2). Receiver operating characteristic (ROC) curves were constructed for both the training and test cohorts. We used bootstrap resampling (n=1000) to determine the area under the curve (AUC) with a 95% confidence interval (CI). The predictive performance of the model in the training and test cohorts was examined via the AUC, accuracy, precision, recall, and F1 score. A logistic regression analysis was employed to establish the clinical model, which was subsequently enhanced by integrating radiomics and clinical features to forge the optimal combined model. Eventually, we elucidated the mechanism of prediction model employing Shapley Additive explanation (SHAP), a cooperative game theory-derived method.[22] The above radiomics analyses were performed via Python (version 3.9.1; www.python.org), simpleitk (version 2.3.1; www.simpleitk.org), pingouin (version 0.5.4; https://pingouin-stats.org), scikit-learn (version 1.4.1; https://scikit-learn.org), xgboost (version 2.0.3; https://xgboost.readthedocs.io), numpy (version 1.26.4; https://numpy.org), pandas (version 2.2.1; https://pandas.pydata.org), matplotlib (version 3.8.3; https://matplotlib.org) and shap (version 0.44.1; https://shap.readthedocs.io) modules, etc.

Statistical Analysis

This study employed SPSS software (version 27.0; IBM Corp, NY, USA) for all statistical analyses. Continuous variables were presented as mean ± standard deviation or median (interquartile range). And categorical variables were expressed as counts and percentages. Those variables were analyzed with Student's *t*-tests/Mann–Whitney *U*-tests or chi-square /Fisher's exact tests, contingent upon the data distribution. Statistical significance was defined as a p value <0.05.

Results

Patient Characteristics and Treatment Response

We retrospectively analyzed 249 patients initially included and selected 115 of them based on the exclusion criteria; the selection process is shown in Figure 1a. According to our observations, no patients achieved CR, 47 achieved PR, 29 achieved SD, and 39 achieved PD. The ORR and DCR were 40.9% and 66.1%, respectively. All patients enrolled were categorized at BCLC stage C or Chinese liver cancer (CNLC) stage IIIa, with ECOG-PS scores of 0 to 2. These patients were then divided 7:3 into a training cohort (n = 80) and a test cohort (n = 35). No difference in baseline characteristics was found between the two cohorts (Table 1). We found that male patients composed 90.4% of the study population, while the majority of patients had a history of HBV infection (n = 100, 87.0%) as well as cirrhosis (n = 90, 78.3%), and 106 patients had tumors with a diameter of >5 cm (Table 1). Supplementary Table S3 summarizes the baseline characteristics of patients in the nonresponse and response groups. Nonresponders presented a higher grade (III + IV) PVTT type (55.4% vs 36.1%, P = 0.009) and larger tumor size (97.1% vs

Table 1 Baseline Characteristics of the Training Cohort and Test Cohort

	Overall Cohort (n = 115)	Training Cohort (n = 80)	Test Cohort (n = 35)	p Value
Demographic Characteristics				
Age, mean ± SD, y	56.1 ± 10.8	56.2 ± 10.8	56.0 ± 11.0	0.912
Gender				0.916
Male, n (%)	104 (90.4)	73 (91.2)	31 (88.6)	
Female, n (%)	11 (9.6)	7 (8.8)	4 (11.4)	
BMI, mean ± SD, kg/m2	22.8 ± 3.2	23.0 ± 3.3	22.2 ± 3.1	0.225
Smoking History				0.91
Yes, n (%)	78 (67.8)	54 (67.5)	24 (68.6)	
No, n (%)	37 (32.2)	26 (32.5)	11 (31.4)	
Drinking History				0.437
Yes, n (%)	75 (65.2)	54 (67.5)	21 (60.0)	
No, n (%)	40 (34.8)	26 (32.5)	14 (40.0)	
HBV Infection				0.522
Yes, n (%)	100 (87.0)	68 (85.0)	32 (91.4)	
No, n (%)	15 (13.0)	12 (15.0)	3 (8.6)	
HCV Infection				1
Yes, n (%)	1 (0.9)	1 (1.3)	0 (0)	
No, n (%)	114 (99.1)	79 (98.7)	35 (100.0)	
NAFLD				/
Yes, n (%)	0 (0)	0 (0)	0 (0)	
No, n (%)	115 (100.0)	80 (100.0)	35 (100.0)	
Cirrhosis				0.096
Yes, n (%)	90 (78.3)	66 (82.5)	24 (68.6)	
No, n (%)	25 (21.7)	16 (17.5)	11 (31.4)	
Clinical Characteristics				
HBV DNA				0.466
≤10^3/mL, n (%)	65 (56.5)	47 (58.8)	18 (51.4)	
>10^3/mL, n (%)	50 (43.5)	33 (41.3)	17 (48.6)	

(*Continued*)

Table 1 (Continued).

	Overall Cohort (n = 115)	Training Cohort (n = 80)	Test Cohort (n = 35)	p Value
AFP				0.702
≤400ng/mL, n (%)	43 (37.4)	29 (36.3)	14 (40.0)	
>400ng/mL, n (%)	72 (62.6)	51 (63.7)	21 (60.0)	
lnAFP, median (IQR), ng/mL	7.0 (4.2, 9.9)	7.1 (4.2, 9.9)	7.0 (3.9, 9.6)	0.765
TBIL, median (IQR), μmol/L	16.0 (12.0, 25.0)	16.0 (11.0, 25.0)	16.0 (12.0, 24.0)	0.801
ALB, mean ± SD, g/L	37.1 ± 4.0	37.0 ± 4.1	37.4 ± 3.9	0.573
ALT, median (IQR), U/L	44.0 (28.0, 71.0)	40.0 (27.0, 66.3)	54.0 (30.0, 79.0)	0.23
AST, median (IQR), U/L	64.0 (46.0, 93.0)	65.5 (44.5, 97.0)	61.0 (51.0, 87.0)	0.985
ALP, median (IQR), U/L	147.0 (117.0, 204.0)	149.5 (114.3, 203.3)	142.0 (119.0, 214.0)	0.908
GGT, median (IQR), U/L	194.0 (127.0, 306.0)	181.5 (120.8, 306.8)	215.0 (127.0, 304.0)	0.555
Neu, median (IQR), 10^9/L	3.6 (2.7, 5.2)	3.5 (2.7, 4.9)	3.8 (2.5, 5.6)	0.402
Lym, median (IQR), 10^9/L	1.1 (0.8, 1.4)	1.1 (0.8, 1.5)	1.1 (0.8, 1.4)	0.944
Mon, median (IQR), 10^9/L	0.4 (0.3, 0.6)	0.5 (0.3, 0.6)	0.4 (0.3, 0.6)	0.932
PLT, median (IQR), 10^9/L	153.0 (114.0, 209.0)	157.5 (110.3, 214.3)	147.0 (116.0, 203.0)	0.777
PT, median (IQR), s	13.8 (13.3, 14.6)	13.9 (13.3, 14.7)	13.7 (13.0, 14.3)	0.293
PLR, median (IQR)	150.0 (96.4, 210.0)	140.8 (96.2, 209.6)	152.5 (105.2, 210.0)	0.939
NLR, median (IQR)	3.3 (2.4, 4.9)	3.2 (2.4, 4.6)	3.5 (2.7, 5.0)	0.292
LMR, median (IQR)	2.5 (1.8, 3.4)	2.5 (1.7, 3.5)	2.5 (1.9, 3.3)	0.798
ALR, median (IQR)	61.9 (37.3, 123.5)	60.4 (36.3, 130.2)	63.8 (39.2, 101.7)	0.851
APR, median (IQR)	0.4 (0.3, 0.7)	0.4 (0.3, 0.7)	0.4 (0.3, 0.7)	0.822
GPR, median (IQR)	1.3 (0.8, 2.5)	1.3 (0.8, 2.5)	1.4 (0.8, 2.6)	0.471
SII, median (IQR)	555.6 (326.2, 760.6)	554.4 (327.9, 749.2)	555.6 (305.0, 986.0)	0.803
ALBI Score, mean ± SD	−2.3 ± 0.4	−2.3 ± 0.4	−2.4 ± 0.4	0.748
Child-Pugh Score				0.36
A (5–6 scores), n (%)	82 (71.3)	55 (68.7)	27 (77.1)	
B (7–9 scores), n (%)	33 (28.7)	25 (31.3)	8 (22.9)	
PVTT Type				0.728
I, n (%)	17 (14.8)	13 (16.2)	4 (11.4)	
II, n (%)	44 (39.3)	28 (35.0)	16 (45.7)	
III, n (%)	39 (33.9)	28 (35.0)	11 (31.4)	
IV, n (%)	15 (13.0)	11 (13.8)	4 (11.4)	
Tumor Number				0.825
Solitary, n (%)	41 (35.7)	28 (35.0)	13 (37.1)	
Multiple, n (%)	74 (64.3)	52 (65.0)	22 (62.9)	
Tumor Size				0.184
≤ 5cm, n (%)	9 (7.8)	4 (5.0)	5 (14.3)	
> 5cm, n (%)	106 (92.2)	76 (95.0)	30 (85.7)	
TACE Type				0.481
C-TACE, n (%)	70 (60.9)	47 (58.8)	23 (65.7)	
D-TACE, n (%)	45 (39.1)	33 (41.3)	12 (34.3)	
Tumor Response				0.485
Response, n (%)	47 (40.9)	31 (38.8)	16 (54.3)	
Nonresponse, n (%)	68 (59.1)	49 (61.2)	19 (45.7)	

Abbreviations: IQR, interquartile range; BMI, body mass index; HBV, hepatitis B virus; HCV, hepatitis C virus; NAFLD, nonalcohol fatty liver disease; HBV DNA, hepatitis B virus DNA copy number; AFP, alpha fetoprotein; T-BIL, total bilirubin; ALB, albumin; ALT, alanine aminotransferase; AST, aspartate aminotransferase; ALP, alkaline phosphatase; GGT, gamma-glutamyl transferase; Neu, neutrophil; Mon, monocyte; Lym, lymphocyte; PLT, platelet; PLR, platelet to lymphocyte ratio; NLR, neutrophil to lymphocyte ratio; LMR, lymphocyte to monocyte ratio; ALR, aspartate aminotransferase to lymphocyte ratio; APR, aspartate aminotransferase to platelet ratio; GPR, gamma-glutamyl transferase to platelet ratio; SII, systemic immune-inflammation index; ALBI, albumin–bilirubin; PVTT, portal vein tumor thrombus; TACE, transarterial chemoembolization; C-TACE, conventional transarterial chemoembolization; D-TACE, drug-eluting beads transcatheter arterial chemoembolization.

85.1%, P = 0.046). The continuous form of the alpha-fetoprotein (AFP) was used for analysis during the clinical feature selection process, as it could provide more information than the categorical form. The variables with P values <0.1 in the univariate analysis included drinking history, the natural logarithm of AFP (InAFP), AST, LMR, ALR, Child–Pugh score, PVTT type, and TACE type. Multivariate logistic regression demonstrated that TACE type was significantly associated with treatment response, and detailed information is provided in Table 2.

Radiomics Feature Selection

Among the radiomics features with ICCs > 0.8 from the three sequences, 12 were retained after dimensionality reduction, and Supplementary Figure S1 presents the process. All radiomics and clinical features are available in Supplementary Table S4.

Table 2 Univariate and Multivariate Analysis of Demographic and Clinical Characteristics

	Univariate Analysis OR (95% CI)	p Value	Multivariate Analysis OR (95% CI)	p Value
Demographic Characteristics				
Age, y	1.007 (0.966–1.050)	0.746		
Gender (Male vs Female)	0.830 (0.173–3.986)	0.816		
BMI, kg/m2	1.023 (0.892–1.174)	0.742		
Smoking History (Yes vs No)	0.500 (0.192–1.299)	0.155		
Drinking History (Yes vs No)	0.394 (0.151–1.030)	0.057	0.739 (0.206–2.659)	0.644
HBV Infection (Yes vs No)	0.581 (0.169–1.998)	0.389		
HCV Infection (Yes vs No)	/	1		
NAFLD (Yes vs No)	/	/		
Cirrhosis (Yes vs No)	1.731 (0.239–2.452)	0.393		
Clinical Characteristics				
HBV DNA (≤10^3/mL vs >10^3/mL)	1.187 (0.474–2.973)	0.714		
AFP (≤400ng/mL vs >400ng/mL)	1.490 (0.588–3.776)	0.401		
InAFP, ng/mL	0.843 (0.718–0.990)	0.038	0.822 (0.675–1.002)	0.052
TBIL, μmol/L	0.990 (0.951–1.032)	0.645		
ALB, g/L	1.050 (0.939–1.175)	0.388		
ALT, U/L	0.997 (0.990–1.004)	0.387		
AST, U/L	0.990 (0.980–1.000)	0.054	0.994 (0.982–1.006)	0.348
ALP, U/L	0.997 (0.992–1.002)	0.283		
GGT, U/L	0.999 (0.996–1.001)	0.299		
Neu, 109/L	0.816 (0.598–1.114)	0.201		
Lym, 109/L	1.425 (0.631–3.221)	0.394		
Mon, 109/L	0.432 (0.049–3.781)	0.448		
PLT, 109/L	0.996 (0.990–1.002)	0.197		
PT, s	1.064 (0.757–1.496)	0.720		
PLR	0.997 (0.991–1.002)	0.231		
NLR	0.942 (0.769–1.155)	0.566		
LMR	1.323 (0.958–1.828)	0.089	1.276 (0.825–1.974)	0.273
ALR	0.994 (0.988–1.001)	0.073	1.001 (0.988–1.013)	0.926
APR	0.670 (0.309–1.456)	0.312		
GPR	1.034 (0.739–1.447)	0.845		
SII	0.999 (0.998–1.000)	0.132		
ALBI Score	0.512 (0.141–1.860)	0.309		
Child-Pugh Score (A vs B)	2.639 (0.914–7.619)	0.073	2.011 (0.561–7.211)	0.283
BCLC Stage	/	/		
PVTT Type (I+II vs III+IV)	2.424 (0.958–6.133)	0.061	1.524 (0.460–5.054)	0.491

(*Continued*)

https://doi.org/10.2147/JHC.S513696

Table 2 (Continued).

	Univariate Analysis OR (95% CI)	p Value	Multivariate Analysis OR (95% CI)	p Value
Tumor Number (Solitary vs Multiple)	2.059 (0.804–5.273)	0.132		
Tumor Size (≤ 5cm vs > 5cm)	5.143 (0.510–51.846)	0.165		
TACE Type (C-TACE vs D-TACE)	0.253 (0.098–0.655)	0.005	0.253 (0.085–0.757)	0.014

Abbreviations: OR, odds ratio; CI, confidence interval; BMI, body mass index; HBV, hepatitis B virus; HCV, hepatitis C virus; NAFLD, nonalcohol fatty liver disease; HBV DNA, hepatitis B virus DNA copy number; AFP, alpha fetoprotein; lnAFP, the natural logarithm of AFP; T-BIL, total bilirubin; ALB, albumin; ALT, alanine aminotransferase; AST, aspartate aminotransferase; ALP, alkaline phosphatase; GGT, gamma-glutamyl transferase; Neu, neutrophil; Mon, monocyte; Lym, lymphocyte; PLT, platelet; PLR, platelet to lymphocyte ratio; NLR, neutrophil to lymphocyte ratio; LMR, lymphocyte to monocyte ratio; ALR, aspartate aminotransferase to lymphocyte ratio; APR, aspartate aminotransferase to platelet ratio; GPR, gamma-glutamyl transferase to platelet ratio; PT, prothrombin time; ALBI, albumin–bilirubin; BCLC, Barcelona Clinic Liver Cancer; CNLC, China liver cancer; PVTT, portal vein tumor thrombus; TACE, transarterial chemoembolization; C-TACE, conventional transarterial chemoembolization; D-TACE, drug-eluting beads transcatheter arterial chemoembolization.

Model Construction and Evaluation

Figure 1b shows the construction and evaluation process of the predictive model, revealing suboptimal clinical model efficacy, with AUCs of 0.66 (95% CI: 0.57–0.76) and 0.41 (95% CI: 0.26–0.55) in the training and test cohorts. We tested four ML classifiers to construct radiomics models. KNN and SVM showed poor predictive performance, perhaps due to overfitting, whereas RF and XGBoost performed better. We evaluated the models on the basis of accuracy, precision, recall, and F1 score and finally chose the RF model after comprehensive consideration. Figure 2 presents the ROC plots and heatmaps of the performance evaluation heatmaps for the four ML models. We also plotted ROC curves for the all models, as displayed in Figure 3a and b. Incorporating clinical variables enhanced the model's predictive performance, achieving AUCs of 0.95 (95% CI: 0.68–0.98) and 0.84 (95% CI: 0.91–0.99). The combined model's metrics in the training cohort were 0.88 accuracy, 0.81 precision, 0.98 recall, and 0.89 F1 score (Figure 3c), surpassing those in the test cohort (0.8, 0.76, 0.81, 0.79; Figure 3d), outperforming the other models.

Model Visualization via SHAP

The "black box" effect of ML makes it difficult to understand how it works.[23] To visualize the output process of the model, we adopted several local explanations to clarify the global structure through SHAP.[22] Figure 4a delineates feature contributions to the model, with "DWI_wavelet-LHL_gldm_HighGrayLevelEmphasis" "T1AP_wavelet-LLH _glcm_Autocorrelation" and "T1AP_wavelet-HLL_firstorder_Range" emerging as the most significant. In addition, we observed that the SHAP value of "T2WI_wavelet-LLH_firstorder_RootMeanSquared" was 0, indicating that this feature had no effect on the model output. Figure 4b reveals each feature's magnitude and distribution of influence on the prediction result. The attribute value of a single feature for each patient in the training cohort matches a single point on the plot. Each feature is sorted by the mean absolute value of its respective SHAP value. Different colors are used to show the original values of features, namely, red for higher values, blue for lower values and intermediate values in purple. The value of the x-axis indicates the direction of the effect of the SHAP value on the model outputs, and a positive value suggests an increased probability of treatment response. As an example, elevated values of feature 9, 2, and 4 indicate a heightened likelihood of response to TACE, lenvatinib, and PD-1 blockade combination therapy. We then randomly selected one responder (Figure 4c) and one nonresponder (Figure 4d) from the training cohort to elucidate the principle more clearly. Figure 4c shows that features 4 and 9 play a positive role, whereas feature 2 has the opposite effect. The final output is 0.83 after the contributions of all the features are integrated, which is consistent with reality. In contrast, as shown in Figure 4d, features 4, 2, and 9 all make a large negative contribution, resulting in a shift of the prediction value to the left of the x-axis, suggesting that this patient is not suitable for combination therapy.

Discussion

To our awareness, this study pioneers radiomics analysis in multidisciplinary therapy for HCC patients with PVTT. We developed a prediction model based on pretreatment contrast-enhanced MRI for evaluating short-term efficacy with

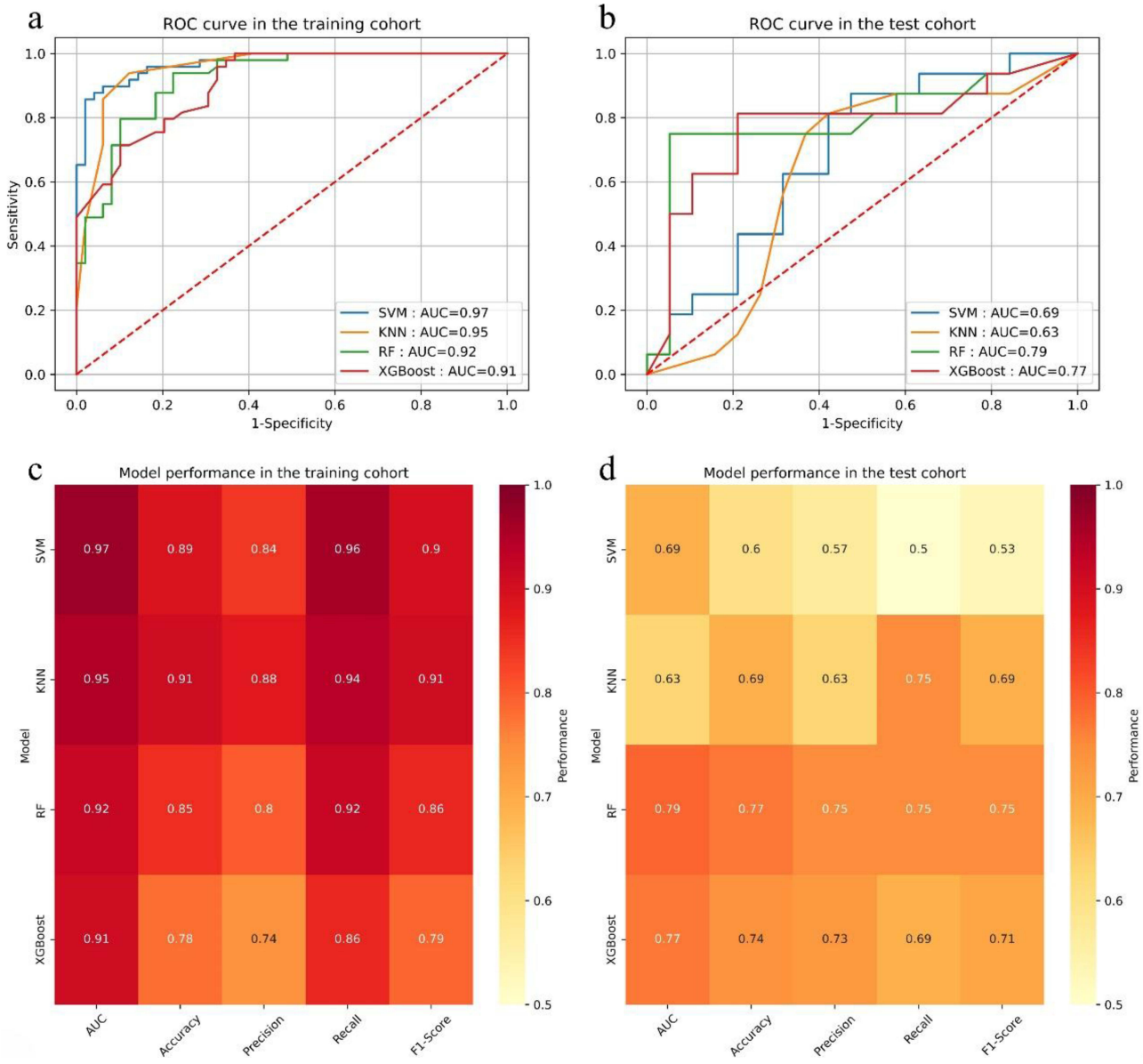

Figure 2 ROC curves and performance evaluation of 4 machine learning radiomics models in the training and test cohorts. (**a**) ROC curves of the ML radiomics models in the training cohort. (**b**) ROC curves of the ML radiomics models in the test cohort. (**c**) Each model performance in the training cohort. (**d**) Each model performance in the test cohort.

satisfactory results. Currently, there is no conclusive evidence on the optimal treatment protocol for HCC-PVTT. European and US guidelines recommend ICIs in combination with antiangiogenic drugs such as bevacizumab and TKIs.[3,4] According to the IMbrave150 study[24] and the KEYNOTE-524 study,[25] this combination therapy achieved better efficacy and longer overall survival. However, endovascular interventions remain the first choice for certain situations in clinical practice in China. TACE combined with systemic therapy has proven safe and effective in HCC-PVTT patients.[26,27] We speculate that the underlying mechanisms are as follows: TACE induces a hypoxic environment while killing tumors and promoting tumor angiogenesis.[28] TKIs have antiangiogenic properties and can effectively inhibit this phenomenon. Additionally, the combination of TACE, TKI and ICI may activate adaptive immunity to regulate the tumor immune microenvironment.[14,27] In this way, combination therapy can achieve synergistic antitumor effects.

The ORR in this study was 40.9%, which is in agreement with previous reports. Nevertheless, owing to tumor heterogeneity, the treatment response varies considerably between patients, and a significant number of patients do not benefit.

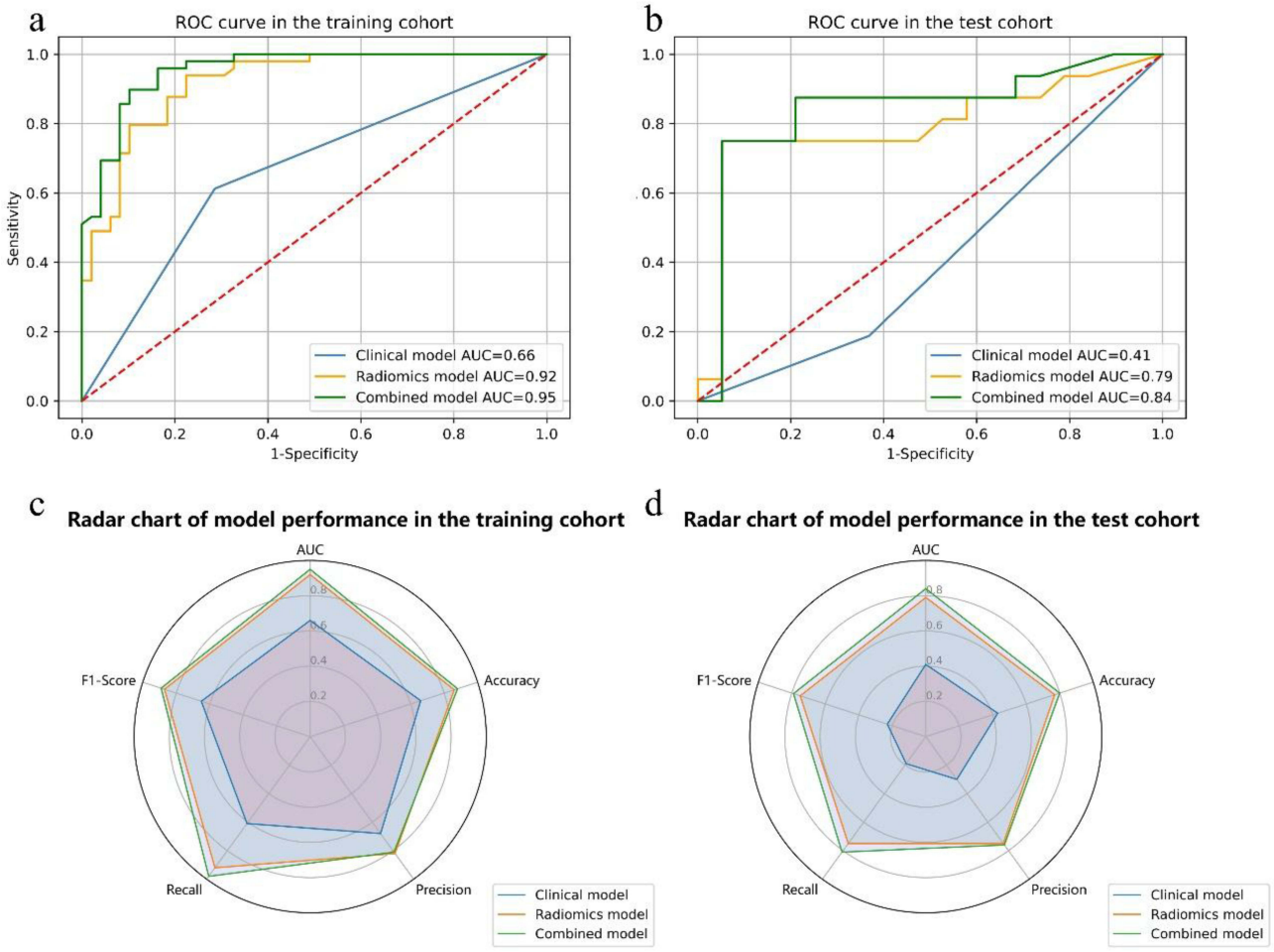

Figure 3 ROC curves performance evaluation of clinical, radiomics and combined models in the training and test cohorts. (**a**) ROC curves of 3 radiomics models in the training cohort. (**b**) ROC curves of the 3 models in the test cohort. (**c** and **d**) Radar chart of model performance in the training and test cohort.

Unrestricted initiation of combination therapy can lead not only to high treatment costs but also to numerous adverse effects, which is clearly contrary to our original intention. As a result, many predictive models have been developed to select patients who are candidates for combination therapy.[12,13,15] Hua et al constructed a radiomics model based on pretreatment CT to identify the population benefiting from lenvatinib plus PD-1 blockade with TACE or HAIC in a noninvasive manner.[13] Compared with CT without ionizing radiation, MRI has higher resolution.[4] A multicenter study assessed the therapeutic efficacy and prognostic implications of lenvatinib paired with anti-PD-1 immunotherapy in advanced HCC patients through MRI radiomics. Researchers have mined deep information hidden behind conventional images, and these high-dimensional features, which are difficult to observe with the naked eye, have more sensitive prognostic relevance.[12]

In our study, 10 of the 12 radiomics features identified after screening were higher-order features obtained via wavelet transform. By definition, the "firstorder_Skewness" feature represents the gray-level distribution of tumor regions in the arterial phase, reflecting the degree of tumor enhancement. Luo et al identified that pretreatment MRI features predict combination therapy efficacy, and reduced arterial enhancement signifies disease progression. In addition, other textural features suggested heterogeneity in signal intensity within the tumor. For example, the "gldm_HighGrayLevelEmphasis" feature represents the extent of high gray level distribution in a given region, emphasizing local heterogeneous information. The "glcm_Autocorrelation" feature, however, is a measure of image texture coarseness, reflecting the spatial correlation of adjacent gray levels. Both of these factors have been confirmed to be correlated with the immune profile of the tumor microenvironment and serve as prognostic factors in non-small cell lung cancer[29] and triple-negative breast cancer.[30]

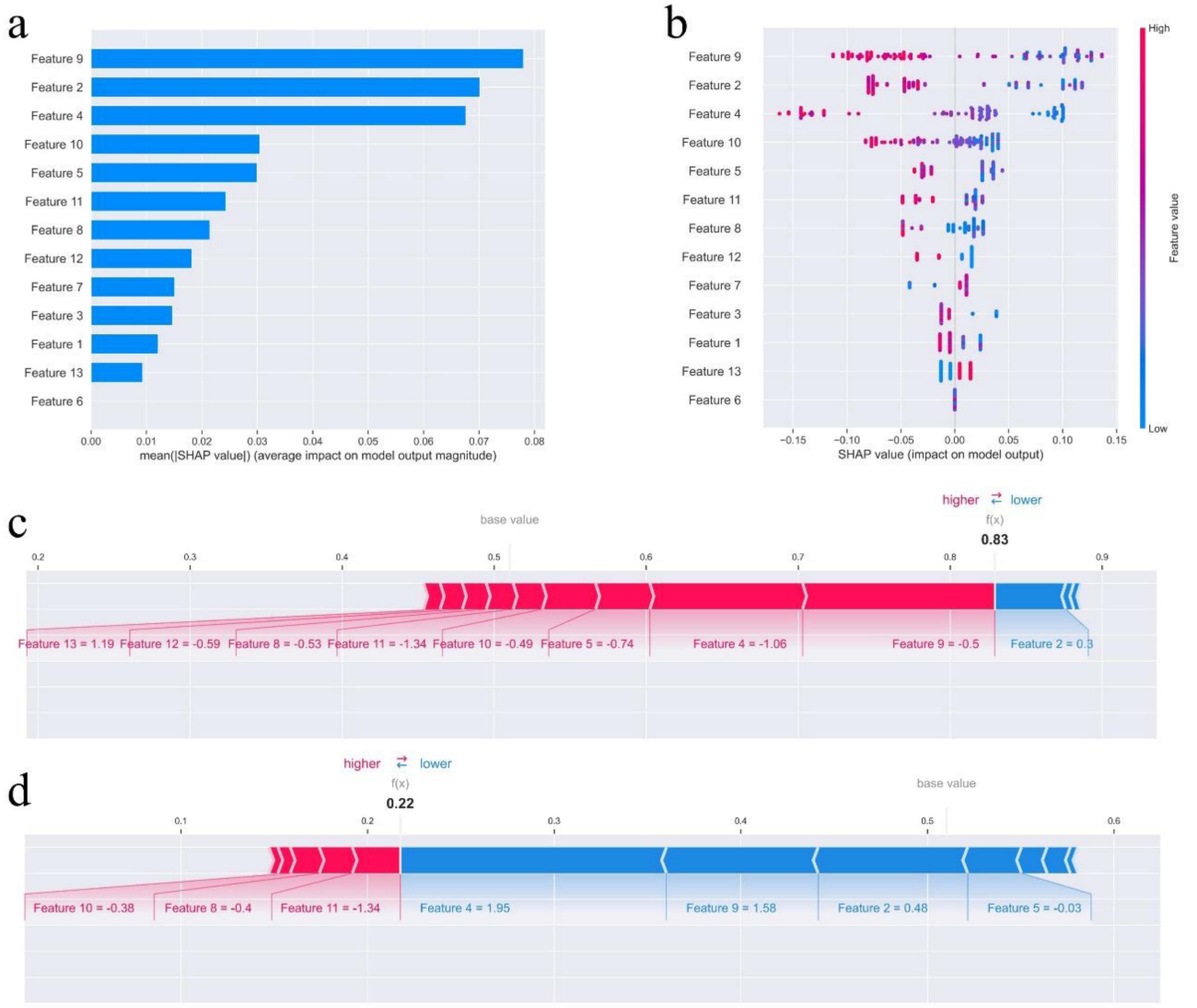

Figure 4 SHAP plot of the combined model. **a** Bar-chart of the average Shapley additive explanation (SHAP) value magnitude displaying features ranked by absolute SHAP value. The larger the average absolute SHAP value of the feature, the more important the feature to the model. **b** SHAP summary plot displaying the magnitude and distribution of the effect of each feature on the model outputs. **c, d** SHAP force plot for the explanation of the model prediction results representing a responder and a non-responder from the training cohort, respectively. The length of the arrow indicates the magnitude of impact, with the red arrows representing an increased probability of response to treatment and the blue representing the opposite result.

Consistent with the majority of findings, the clinical model failed to show good predictive performance.[12,13,15,16] In this study, the predictive model was built via logistic regression using a single clinical variable, with low AUC values (0.66, 0.41), whereas the radiomics and combined models performed well. In this study, a predictive model was established using a single clinical variable through logistic regression, with low AUC values (0.66, 0.41), whereas the radiomics and combined models performed well. Notably, our study considered TACE type as an independent clinical predictor, and patients treated with DEB-TACE plus systemic therapy responded better. However, this conclusion seems to be controversial. Compared with conventional TACE, DEB-TACE did not significantly improve long-term survival in advanced HCC patients with PVTT.[31] Moreover, there is no clear evidence of superiority between conventional TACE and DEB-TACE. Further prospective clinical studies are therefore needed in the future to draw conclusions. In addition, PVTT type may be associated with treatment efficacy according to univariate logistic regression but was excluded from multivariate analyses. During the baseline characteristic analysis, we found a greater proportion of responders with PVTT types I and II than nonresponders (63.9% vs 45.6%, P = 0.009). Similarly, two retrospective studies indicated that patients with high-grade PVTT who underwent TACE with lenvatinib plus PD-1 inhibitors had a worse prognosis.[32,33]

ML models are increasingly being applied to solve scientific problems. Owing to the opaque decision-making process, users have no insight into the internal logic and operational processes, only the model input and output.[23] For clinicians, blind faith in the model output in clinical practice is poor, and attention should also be given to interpretability.[22] SHAP is a practical and efficient ML interpretation tool that can clearly demonstrate local effects and overall impacts to support clinical decision-making.[22,34] Thirteen variables were used to develop the combined model, and SHAP plots highlighted the three most important variables, namely, "DWI_wavelet-LHL_gldm_HighGrayLevelEmphasis", "T1AP_wavelet-LLH_glcm_Autocorrelation" and "T1AP_wavelet-HLL_firstorder_Range". The SHAP force plot then displays the individualized prediction process, increasing transparency and comprehension to further guide clinical diagnosis and treatment.

There are several limitations of this study. First, the sample sizes collected from the two institutions were limited, and an independent external validation cohort has not yet been established to test the accuracy and generalizability of the model. This was a retrospective study with inevitable selection bias. For example, the study cohort predominantly comprised HBV-infected individuals; the REFLECT trial's Chinese subgroup indicated that lenvatinib may be particularly efficacious for hepatitis B-related HCC.[35] However, the etiological heterogeneity of HCC results in wide variations in efficacy and prognosis.[36] This raises the critical question of whether distinct etiological of HCC exhibit differential associations with radiomics features – a hypothesis meriting systematic investigation. A recent study revealed that GLCM and GLDM features in the hepatobiliary phase of gadoxetic acid-enhanced MRI exhibit correlations with HCC development in HBV-infected patients.[37] However, the exclusive reliance on a single imaging phase potentially diminishes the broader applicability of the conclusion. Additionally, researchers explored the feasibility of gadoxetic acid-enhanced MRI radiomics for predicting etiological subtypes of liver cirrhosis, demonstrating promising diagnostic potential.[38] Nevertheless, limitations such as restricted sample size and intergroup imbalance urgently require resolution. Thus, there is an urgent need for further large, multicenter prospective studies to confirm these findings. The establishment of a public image management platform across regions and ethnicities may help advance related research. Second, there is a lack of standards for MRI acquisition equipment, parameters and image segmentation, which may lead to measurement differences in image features. Although we performed image preprocessing, the effects of these methods in abdominal examination have not been proven at this time. Moreover, ROI segmentation was achieved manually and relied on subjective judgment. Third, we performed only a single omics analysis and may have ignored the biological background. Multiomics studies that integrate macroscopic radiomics, microscopic pathomics and genomics can enhance biological interpretation and help assess disease progression and treatment response.

Conclusion

This study elucidated the association between MRI radiomics and multidisciplinary treatment outcomes in HCC-PVTT patients. Furthermore, we successfully established and validated a noninvasive predictive model based on radiomics and clinical indicators to screen for the appropriate population to receive triple TLP therapy. The operation principle was explained through SHAP both locally and globally.

Abbreviations

AFP, Alpha-fetoprotein; AUC, Area under the curve; BCLC, Barcelona Clinic Liver Cancer; CI, confidence interval; CNLC, Chinese liver cancer; CR, Complete response; DCR, Disease control rate; DEB, Drug-eluting bead; DICOM, Digital imaging and communications in medicine; DWI, Diffusion-weighted imaging; ECOG-PS, Eastern Cooperative Oncology Group performance status; GLCM, Gray level co-occurrence matrix texture; GLDM, Gray level dependence matrix; GLRLM, Gray level run length matrix; GLSZM, Gray level size zone matrix; HCC, Hepatocellular carcinoma; ICC, Intraclass correlation coefficient; KNN, k-nearest neighbor; LASSO, Least absolute shrinkage and selection operator; ML, Machine learning; mRECIST, modified Response Evaluation Criteria in Solid Tumors; NGTDM, neighboring gray tone difference matrix; ORR, Objective response rate; PD-1, Programmed cell death protein 1; PD, Progressive disease; PR, Partial response; PVTT, Portal vein tumor thrombus; RF, random forest; RFE, Recursive feature elimination; ROC, Receiver operating characteristic; ROI, Region of interest; SD, Stable disease; SHAP, Shapley Additive explanation; SMOTE, Synthetic minority oversampling

technique; SVM, support vector machine; T1WI, T1-weighted imaging; T2WI, T2-weighted imaging; TACE, Transarterial chemoembolization; XGBoost, eXtreme gradient boosting.

Data Sharing Statement

Date will be made available on request.

Ethics Approval and Informed Consent

This study was conducted in accordance with the principles of the Declaration of Helsinki and was approved by the Ethics Committee of the First Affiliated Hospital of Wenzhou Medical University and the Fifth Affiliated Hospital of Wenzhou Medical University. Written informed consent was waived because of the retrospective nature of the study. To ensure confidentiality, all patients' information was subjected to anonymization.

Funding

This study was Supported by the National Natural Science Foundation of China (Grant No. 81972233), Major scientific and technological innovation project of Wenzhou Science and Technology Bureau (Grant No. ZY2021009), Shanghai Clinical Research Center for Interventional Medicine (No.19MC1910300).

Disclosure

The authors report no conflicts of interest in this work.

References

1. Bray F, Laversanne M, Sung H, et al. Global cancer statistics 2022: GLOBOCAN estimates of incidence and mortality worldwide for 36 cancers in 185 countries. *CA Cancer J Clin*. 2024;74(3):229–263. doi:10.3322/caac.21834
2. Sun J, Guo R, Bi X, et al. Guidelines for Diagnosis and Treatment of Hepatocellular Carcinoma with Portal Vein Tumor Thrombus in China (2021 Edition). *Liver Cancer*. 2022;11(4):315–328. doi:10.1159/000523997
3. Reig M, Forner A, Rimola J, et al. BCLC strategy for prognosis prediction and treatment recommendation: the 2022 update. *J Hepatol*. 2022;76 (3):681–693. doi:10.1016/j.jhep.2021.11.018
4. Singal AG, Llovet JM, Yarchoan M, et al. AASLD Practice Guidance on prevention, diagnosis, and treatment of hepatocellular carcinoma. *Hepatology*. 2023;78(6):1922–1965. doi:10.1097/HEP.0000000000000466
5. Zhou J, Sun H, Wang Z, et al. Guidelines for the Diagnosis and Treatment of Primary Liver Cancer (2022 Edition). *Liver Cancer*. 2023;12 (5):405–444. doi:10.1159/000530495
6. Xiang X, Lau WY, Wu ZY, et al. Transarterial chemoembolization versus best supportive care for patients with hepatocellular carcinoma with portal vein tumor thrombus: a multicenter study. *Eur J Surg Oncol*. 2019;45(8):1460–1467. doi:10.1016/j.ejso.2019.03.042
7. Ding X, Sun W, Li W, et al. Transarterial chemoembolization plus lenvatinib versus transarterial chemoembolization plus sorafenib as first-line treatment for hepatocellular carcinoma with portal vein tumor thrombus: a prospective randomized study. *Cancer*. 2021;127(20):3782–3793. doi:10.1002/cncr.33677
8. Li X, Ding X, Liu M, et al. A multicenter prospective study of TACE combined with lenvatinib and camrelizumab for hepatocellular carcinoma with portal vein tumor thrombus. *Cancer Med*. 2023;12(16):16805–16814. doi:10.1002/cam4.6302
9. Lambin P, Rios-Velazquez E, Leijenaar R, et al. Radiomics: extracting more information from medical images using advanced feature analysis. *Eur J Cancer*. 2012;48(4):441–446. doi:10.1016/j.ejca.2011.11.036
10. Mayerhoefer ME, Materka A, Langs G, et al. Introduction to Radiomics. *J Nucl Med*. 2020;61(4):488–495. doi:10.2967/jnumed.118.222893
11. Bo Z, Chen B, Zhao Z, et al. Prediction of Response to Lenvatinib Monotherapy for Unresectable Hepatocellular Carcinoma by Machine Learning Radiomics: a Multicenter Cohort Study. *Clin Cancer Res*. 2023;29(9):1730–1740. doi:10.1158/1078-0432.CCR-22-2784
12. Xu B, Dong SY, Bai XL, et al. Tumor Radiomic Features on Pretreatment MRI to Predict Response to Lenvatinib plus an Anti-PD-1 Antibody in Advanced Hepatocellular Carcinoma: a Multicenter Study. *Liver Cancer*. 2022;12(3):262–276. doi:10.1159/000528034
13. Hua Y, Sun Z, Xiao Y, et al. Pretreatment CT-based machine learning radiomics model predicts response in unresectable hepatocellular carcinoma treated with lenvatinib plus PD-1 inhibitors and interventional therapy. *J Immunother Cancer*. 2024;12(7):e008953. doi:10.1136/jitc-2024-008953
14. Zhao Y, Zhang YN, Wang KT, et al. Lenvatinib for hepatocellular carcinoma: from preclinical mechanisms to anti-cancer therapy. *Biochim Biophys Acta Rev Cancer*. 2020;1874(1):188391. doi:10.1016/j.bbcan.2020.188391
15. Luo J, Huang Z, Wang M, Li T, Huang J. Prognostic role of multiparameter MRI and radiomics in progression of advanced unresectable hepatocellular carcinoma following combined transcatheter arterial chemoembolization and lenvatinib therapy. *BMC Gastroenterol*. 2022;22 (1):108. doi:10.1186/s12876-022-02129-9
16. Cheng S, Hu G, Jin Z, Wang Z, Xue H. CT-based radiomics nomogram for prediction of survival after transarterial chemoembolization with drug-eluting beads in patients with hepatocellular carcinoma and portal vein tumor thrombus. *Eur Radiol*. 2023;33(12):8715–8726. doi:10.1007/s00330-023-09830-7
17. Shi J, Lai EC, Li N, et al. A new classification for hepatocellular carcinoma with portal vein tumor thrombus. *J Hepatobiliary Pancreat Sci*. 2011;18(1):74–80. doi:10.1007/s00534-010-0314-0

18. Li S, Wu J, Wu J, et al. Prediction of early treatment response to the combination therapy of TACE plus lenvatinib and anti-PD-1 antibody immunotherapy for unresectable hepatocellular carcinoma: multicenter retrospective study. *Front Immunol*. 2023;14:1109771. doi:10.3389/fimmu.2023.1109771
19. Lencioni R, Llovet JM. Modified RECIST (mRECIST) assessment for hepatocellular carcinoma. *Semin Liver Dis*. 2010;30(1):52–60. doi:10.1055/s-0030-1247132
20. Moradmand H, Aghamiri SMR, Ghaderi R. Impact of image preprocessing methods on reproducibility of radiomic features in multimodal magnetic resonance imaging in glioblastoma. *J Appl Clin Med Phys*. 2020;21(1):179–190. doi:10.1002/acm2.12795
21. Tustison NJ, Avants BB, Cook PA, et al. N4ITK: improved N3 bias correction. *IEEE Trans Med Imag*. 2010;29(6):1310–1320. doi:10.1109/TMI.2010.2046908
22. Lundberg SM, Erion G, Chen H, et al. From Local Explanations to Global Understanding with Explainable AI for Trees. *Nat Mach Intell*. 2020;2(1):56–67. doi:10.1038/s42256-019-0138-9
23. Bo Z, Song J, He Q, et al. Application of artificial intelligence radiomics in the diagnosis, treatment, and prognosis of hepatocellular carcinoma. *Comput Biol Med*. 2024;173:108337. doi:10.1016/j.compbiomed.2024.108337
24. Finn RS, Qin S, Ikeda M, et al. Atezolizumab plus bevacizumab in unresectable hepatocellular carcinoma. *N Engl J Med*. 2020;382(20):1894–1905. doi:10.1056/NEJMoa1915745
25. Finn RS, Ikeda M, Zhu AX, et al. Phase Ib Study of Lenvatinib Plus Pembrolizumab in Patients With Unresectable Hepatocellular Carcinoma. *J Clin Oncol*. 2020;38(26):2960–2970. doi:10.1200/JCO.20.00808
26. Wu HX, Ding XY, Xu YW, et al. Transcatheter arterial chemoembolization combined with PD-1 inhibitors and Lenvatinib for hepatocellular carcinoma with portal vein tumor thrombus. *World J Gastroenterol*. 2024;30(8):843–854. doi:10.3748/wjg.v30.i8.843
27. Yang F, Xu GL, Huang JT, et al. Transarterial Chemoembolization Combined With Immune Checkpoint Inhibitors and Tyrosine Kinase Inhibitors for Unresectable Hepatocellular Carcinoma: efficacy and Systemic Immune Response. *Front Immunol*. 2022;13:847601. doi:10.3389/fimmu.2022.847601
28. Virmani S, Rhee TK, Ryu RK, et al. Comparison of hypoxia-inducible factor-1alpha expression before and after transcatheter arterial embolization in rabbit VX2 liver tumors. *J Vasc Interv Radiol*. 2008;19(10):1483–1489. doi:10.1016/j.jvir.2008.06.017
29. Trentini F, Mazzaschi G, Milanese G, et al. Validation of a radiomic approach to decipher NSCLC immune microenvironment in surgically resected patients. *Tumori*. 2022;108(1):86–92. doi:10.1177/03008916211000808
30. Yu H, Meng X, Chen H, et al. Correlation Between Mammographic Radiomics Features and the Level of Tumor-Infiltrating Lymphocytes in Patients With Triple-Negative Breast Cancer. *Front Oncol*. 2020;10:412. doi:10.3389/fonc.2020.00412
31. Gorodetski B, Chapiro J, Schernthaner R, et al. Advanced-stage hepatocellular carcinoma with portal vein thrombosis: conventional versus drug-eluting beads transcatheter arterial chemoembolization. *Eur Radiol*. 2017;27(2):526–535. doi:10.1007/s00330-016-4445-9
32. Zou X, Xu Q, You R, Yin G. Evaluating the Benefits of TACE Combined with Lenvatinib Plus PD-1 Inhibitor for Hepatocellular Carcinoma with Portal Vein Tumor Thrombus. *Adv Ther*. 2023;40(4):1686–1704. doi:10.1007/s12325-023-02449-6
33. Zou X, Xu Q, You R, Yin G. Correlation and efficacy of TACE combined with lenvatinib plus PD-1 inhibitor in the treatment of hepatocellular carcinoma with portal vein tumor thrombus based on immunological features. *Cancer Med*. 2023;12(10):11315–11333. doi:10.1002/cam4.5841
34. Ma J, Bo Z, Zhao Z, et al. Machine Learning to Predict the Response to Lenvatinib Combined with Transarterial Chemoembolization for Unresectable Hepatocellular Carcinoma. *Cancers*. 2023;15(3):625. doi:10.3390/cancers15030625
35. Kudo M, Finn RS, Qin S, et al. Lenvatinib versus sorafenib in first-line treatment of patients with unresectable hepatocellular carcinoma: a randomised Phase 3 non-inferiority trial. *Lancet*. 2018;391(10126):1163–1173. doi:10.1016/S0140-6736(18)30207-1
36. Barcena-Varela M, Lujambio A. The Endless Sources of Hepatocellular Carcinoma Heterogeneity. *Cancers*. 2021;13(11):2621. doi:10.3390/cancers13112621
37. Tang M, Xu D, Jin H, et al. Prediction of the early hepatocellular carcinoma development in patients with chronic hepatitis B virus infection using gadoxetic acid-enhanced magnetic resonance imaging. *BMC Cancer*. 2024;24(1):1425. doi:10.1186/s12885-024-13185-7
38. Elkilany A, Fehrenbach U, Auer TA, et al. A radiomics-based model to classify the etiology of liver cirrhosis using gadoxetic acid-enhanced MRI. *Sci Rep*. 2021;11(1):10778. doi:10.1038/s41598-021-90257-9